IJER 5(1) October (2026) pages 47-67

International Journal of Engineering Research

Sirte University

Faculty of Engineering

Journal homepage: Scientific Journals (su.edu.ly)

Sliding Mode Controller of Quadcopter for Altitude Regulation and Square Trajectory Tracking

Khalfallh A. E. Husain

Electrical and Electronics Department, Faculty of Engineering, Sirte University, Sirte, Libya.

Corresponding Author: khalfhusain@su.edu.ly

ARTICLE INFOR

Article history:

Received 20 September 2026

Revised 15 October 2026

Accepted 22 October 2026

Available online

1 November 2026

ABSTRACT

In recent years, Unmanned Aerial Vehicles (UAVs), particularly quadrotor systems, have attracted considerable research interest owing to their vertical takeoff and landing capabilities, agility, and versatility in applications ranging from surveillance and environmental monitoring to search and rescue missions. The quadcopter is modeled as a six-degree-of-freedom (6-DOF) rigid body system with four rotors. Its dynamics are inherently nonlinear and strongly coupled, influenced by thrust forces, torques, gravitational forces, and aerodynamic effects. The Newton–Euler formulation is used to derive the translational and rotational equations of motion.

This research introduced sliding mode controller to overcome suffering limitation of conventional PID controller. The simulation using matlab Simulink library and codes to simulate the proposed model.

Simulation results are presented to validate the effectiveness of the proposed controller, highlighting improvements in trajectory tracking accuracy, robustness, and overall flight stability.

2025 Sirte University, All rights are reserved

Keywords: *quadcopter, sliding mode control, altitude control, square trajectory tracking.*

1. Introduction

Unmanned Aerial Vehicles (UAVs), particularly quadcopters, have gained widespread attention in recent years due to their vertical takeoff and landing capabilities, agility, and versatility in applications ranging from surveillance and environmental monitoring to search and rescue missions. Despite their advantages, quadcopters are inherently nonlinear, strongly coupled, and highly sensitive to external disturbances such as wind gusts and payload variations [1]. These characteristics make accurate altitude regulation and trajectory tracking a challenging control problem.

Conventional control techniques, particularly Proportional–Integral–Derivative (PID) controllers, are widely adopted in UAV applications because of their straightforward design and relatively simple implementation. Nevertheless, their control performance may deteriorate in the presence of pronounced system nonlinearities and external disturbances that vary over time, which can reduce their reliability under challenging flight conditions [2].

To overcome these limitations, Sliding Mode Control (SMC) has been widely studied for quadcopter systems because of its robustness against uncertainties and external disturbances. SMC ensures system stability by driving the states to a predefined sliding surface using a high-gain switching control law, typically analyzed through Lyapunov-based methods [3,4].

2. Related Work

Quadcopter altitude and attitude control have received significant attention because of the system's nonlinear dynamics, coupling effects, and sensitivity to external disturbances. Classical control methods, especially Proportional–Integral–Derivative (PID) controllers, have been widely used due to their simple structure and ease of implementation. In [2], advanced tuning techniques such as the Cohen–Coon method were applied to improve system response, stability, and disturbance rejection compared with conventional PID tuning methods. In addition, a nonlinear mathematical model based on the Newton–Euler formulation was developed to describe quadcopter dynamics accurately, and a PID controller was designed for altitude regulation while assuming stable attitude dynamics [5].

Simulation results in MATLAB/Simulink showed that PID controllers can provide satisfactory altitude tracking with small overshoot and stable hovering performance. The controller was also capable of tracking time-varying reference signals with

acceptable accuracy. However, PID-based methods may suffer from reduced performance under strong nonlinearities and external disturbances.

To address these limitations, advanced nonlinear control techniques such as Sliding Mode Control (SMC) have been widely investigated. SMC provides strong robustness against uncertainties and disturbances while ensuring system stability using Lyapunov-based design methods [1], [4]. Nevertheless, conventional SMC may introduce chattering effects, which can reduce control smoothness and affect system performance.

Several improved SMC approaches have been proposed to reduce chattering and enhance robustness. These include higher-order methods such as Super-Twisting SMC and hybrid PID-SMC controllers that improve tracking accuracy and disturbance rejection [6]. Observer-based techniques, including the Extended State Observer (ESO), have also been combined with SMC to estimate and compensate for disturbances in real time, reducing the requirement for high control gains and improving overall system stability [3].

Furthermore, adaptive and intelligent control methods such as adaptive backstepping control, fractional-order SMC, and neural network-based controllers have been introduced to improve adaptability and tracking performance under uncertain operating conditions [7], [8]. More advanced methods, including terminal sliding mode control combined with quaternion-based representations, were proposed to achieve finite-time convergence and avoid singularities in attitude control systems [9].

Despite these developments, challenges still remain regarding controller complexity, computational cost, and practical implementation. Therefore, achieving a balance between simplicity, robustness, and high tracking performance continues to be an important research direction in quadcopter control systems.

3. Research Gap and Contribution

Although many advanced control strategies have been proposed for quadcopter systems, most of these methods involve high computational complexity and difficult implementation, which reduce their suitability for practical applications. On the other hand, conventional controllers such as PID are simple and easy to implement but may not provide sufficient robustness against nonlinearities, parameter uncertainties, and external disturbances. Therefore, this study proposes a Sliding Mode Control (SMC) approach for quadcopter altitude regulation and trajectory tracking along a square path in the x-direction. The proposed controller utilizes the

robustness and disturbance-rejection capability of SMC to improve system stability and tracking performance under uncertain operating conditions. The main contributions of this work include simplifying the quadcopter mathematical model, achieving accurate altitude stabilization in the presence of external disturbances, ensuring precise trajectory tracking along a square path, and comparing the performance of conventional controllers with the proposed SMC approach.

4. Methodology

The research methodology is based on modeling the quadcopter system using the Newton–Euler equations to describe the vehicle dynamics. After developing the mathematical model, a Sliding Mode Controller (SMC) is designed to control the quadcopter altitude and track motion along the X-direction following a predefined path. MATLAB/Simulink simulations are used to evaluate the controller performance, and the obtained results are compared with those of the conventional PID controller in terms of stability, tracking accuracy, and disturbance rejection.

4.1. Modeling of Quadcopter System:

In this study, the quadcopter's orientation is described using Euler angles, namely roll (ϕ), pitch (θ), and yaw (ψ). The transformation between the inertial(earth) and body frames is represented by rotation matrices. By combining the rotations about the three coordinate axes, the overall rotation matrix is obtained and used to transform vectors between the two reference frames [5]. The rotational relationship between the body-fixed and inertial reference frames is illustrated in Fig. 1, while the corresponding trigonometric expressions and transformation matrices are presented in Equation (1).

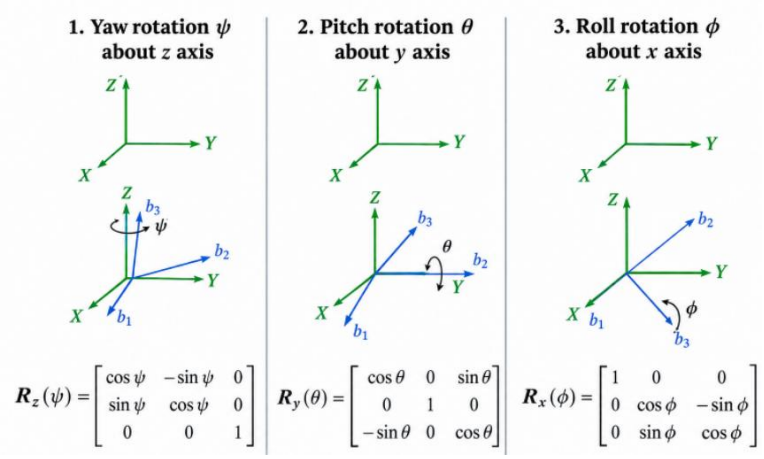


Fig. 1. Rotation of the body-frame axes with respect to the corresponding inertial-frame axes.

$$\begin{bmatrix} b_1 \\ b_2 \\ b_3 \end{bmatrix} = \begin{bmatrix} 1 & 0 & 0 \\ 0 & \mathrm{cs}\,\phi & \mathrm{sn}\,\phi \\ 0 & -\mathrm{sn}\,\phi & \mathrm{cs}\,\phi \end{bmatrix} \begin{bmatrix} \mathrm{cs}\,\theta & 0 & -\mathrm{sn}\,\theta \\ 0 & 1 & 0 \\ \mathrm{sn}\,\theta & 0 & \mathrm{cs}\,\theta \end{bmatrix} \begin{bmatrix} \mathrm{cs}\,\psi & \mathrm{sn}\,\psi & 0 \\ -\mathrm{sn}\,\psi & \mathrm{cs}\,\psi & 0 \\ 0 & 0 & 1 \end{bmatrix} \begin{bmatrix} x \\ y \\ z \end{bmatrix} \quad (1)$$

By multiplying the three rotation matrices, a single transformation matrix R^b is obtained:

$$\begin{bmatrix} b_1 \\ b_2 \\ b_3 \end{bmatrix} \begin{bmatrix} \mathrm{cs}\,\theta\,\mathrm{cs}\,\psi & \mathrm{cs}\,\theta\,\mathrm{sn}\,\psi & -\mathrm{sn}\,\theta \\ -\mathrm{cs}\,\phi\,\mathrm{sn}\,\psi + \mathrm{cs}\,\psi\,\mathrm{sn}\,\theta\,\mathrm{sn}\,\phi & \mathrm{cs}\,\psi\,\mathrm{cs}\,\phi + \mathrm{sn}\,\theta\,\mathrm{sn}\,\phi\,\mathrm{sn}\,\psi & \mathrm{cs}\,\theta\,\mathrm{sn}\,\phi \\ \mathrm{sn}\,\psi\,\mathrm{sn}\,\phi + \mathrm{cs}\,\psi\,\mathrm{cs}\,\phi\,\mathrm{sn}\,\theta & -\mathrm{sn}\,\phi\,\mathrm{cs}\,\psi + \mathrm{cs}\,\phi\,\mathrm{sn}\,\theta\,\mathrm{sn}\,\psi & \mathrm{cs}\,\theta\,\mathrm{cs}\,\phi \end{bmatrix} \begin{bmatrix} x \\ y \\ z \end{bmatrix} (2)$$

The transformation from the body frame to the inertial frame can be obtained using the inverse of the transformation matrix, hence R^i is

$$\begin{bmatrix} x \\ y \\ z \end{bmatrix} \begin{bmatrix} \mathrm{cs}\,\theta\,\mathrm{cs}\,\psi & -\mathrm{cs}\,\phi\,\mathrm{sn}\,\psi + \mathrm{cs}\,\psi\,\mathrm{sn}\,\theta\,\mathrm{sn}\,\phi & \mathrm{sn}\,\psi\,\mathrm{sn}\,\phi + \mathrm{cs}\,\psi\,\mathrm{cs}\,\phi\,\mathrm{sn}\,\theta \\ \mathrm{cs}\,\theta\,\mathrm{sn}\,\psi & \mathrm{cs}\,\psi\,\mathrm{cs}\,\phi + \mathrm{sn}\,\theta\,\mathrm{sn}\,\phi\,\mathrm{sn}\,\psi & -\mathrm{sn}\,\phi\,\mathrm{cs}\,\psi + \mathrm{cs}\,\phi\,\mathrm{sn}\,\theta\,\mathrm{sn}\,\psi \\ -\mathrm{sn}\,\theta & \mathrm{cs}\,\theta\,\mathrm{sn}\,\phi & \mathrm{cs}\,\theta\,\mathrm{cs}\,\phi \end{bmatrix} \begin{bmatrix} b_1 \\ b_2 \\ b_3 \end{bmatrix} (3)$$

Where: $\mathrm{cs}\,\theta$ is $\cos\theta$, and $\mathrm{sn}\,\theta$ is $\sin\theta$.

4.1.1. Newton's Second Law of Motion

The mathematical models describing the translational and rotational behavior of the system in Equation (4) are established based on Newton's second law of motion. This fundamental principle indicates that the resultant external force acting on an object corresponds to the time derivative of its linear momentum [5]. For a body of constant mass, this principle can be represented mathematically as:

$$F = \frac{dP}{dt} = m\frac{dV}{dt} = ma \qquad (4)$$

In rotational motion, the angular momentum of a rigid body is determined by the cross product of its position vector and linear momentum. Accordingly, the angular momentum can be written as:

$$H = \vec{r} \times F = \vec{r} \times m\frac{dV}{dt} \qquad (5)$$

The rotational effect produced by an applied force is described by the moment (torque), which is defined as the time rate of change of angular momentum. Therefore, the governing relationship is expressed as:

$$M = \frac{dH}{dt} \qquad (6)$$

For rotation about a fixed axis, this relationship can be simplified to:

$$M = I\frac{d\omega}{dt} = I\dot{\omega} \qquad (7)$$

Where F denotes the resultant applied force, P represents linear momentum, m is the mass of the vehicle, and a denotes its linear acceleration. Furthermore,Vrepresents linear velocity, $\vec{r}$ is the position vector, and H denotes angular momentum. The rotational quantities -include$M$, representing the applied moment,I, denoting the moment of inertia about the considered axis, ω, representing angular velocity, and $\dot{\omega}$, indicating angular acceleration.

4.1.2. Thrust Equations

The thrust generated by each of the four motors is mathematically expressed by the corresponding equations presented in Equations (8)–(11).

-Vertical thrust.

$$U1 = b(w_1^2 + w_2^2 + w_3^2 + w_4^2) \qquad (8)$$

-Roll thrust.

$$U2 = bsin(\tfrac{pi}{4})(w_1^2 - w_2^2 - w_3^2 + w_4^2) \qquad (9)$$

-Pitch thrust.

$$U3 = bsin(\tfrac{pi}{4})(-w_1^2 - w_2^2 + w_3^2 + w_4^2) \qquad (10)$$

-Yaw thrust.

$$U4 = d(w_1^2 - w_2^2 + w_3^2 - w_4^2) \qquad (11)$$

The combined angular velocity of the four propellers is determined mathematically using Equation (12).

$$\omega_5 = \omega_1 - \omega_2 + \omega_3 - \omega_4 \qquad (12)$$

4.1.3. Moments of Inertia

The moment of inertia represents the resistance of the quadcopter to rotational motion. For a symmetrical vehicle, the moments of inertia about the three axes are described as follows:

$$I = \begin{bmatrix} I_{xx} & 0 & 0 \\ 0 & I_{yy} & 0 \\ 0 & 0 & I_{zz} \end{bmatrix} \qquad (13)$$

$I_{xx}, I_{yy}\ and\ I_{zz}$ represent the moments of inertia about the principal axes of the body frame. Since quadcopters usually operate at low altitudes, the air density is assumed to remain constant during operation [5].

$$I_{zz} = \left(\frac{1}{3} \times \frac{M}{4} \times l^2\right) \times 4 \qquad (14)$$

$$I_{zz} = (\frac{1}{3} \times \frac{0.944}{4} \times 0.230^2) \times 4$$

$$I_{zz} = 0.0166 kgm^2$$

$$I_{xx} = I_{yy} = 0.0071 kgm^2 \qquad (15)$$

Where: $m = mass\ of\ vhical$=0.944kg and l=length of vehicle=0.230m.

To estimate the propeller moment of inertia, one half of the propeller is divided into three sections, as illustrated in Fig. 2.

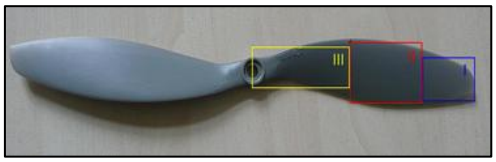


Fig.2: Propeller divided into three parts.

The moment of inertia of each section is then calculated using equation (16) and equation (17), and the total propeller moment of inertia(I_p), table (1), is obtained by summing the contributions of all sections [5].

$$I = m((\frac{h^2}{12}) + (\frac{w^2}{12})) \qquad (16)$$

$$I_p = 2(I_1 + I_2 + I_3) \qquad (17)$$

Table 1: Propeller's parts properties

Part	Mass(g)	Width(cm)	Height(cm)	r(cm),distance from the shaft
I	1.7	3	2.5	9
II	2.6	4.4	2.8	5
III	1.2	5	1.2	0
Ip	$4.439*10^{-5} kgm^3$			

4.1.4. Thrust Coefficient

Under steady-state hovering conditions, the quadcopter maintains equilibrium when the combined thrust generated by its four rotors counteracts the gravitational force acting on the vehicle. Assuming an equal distribution of the lifting force among all rotors, each motor is required to generate a thrust equivalent to one-fourth of the

vehicle's total weight [5,6]. According to the aerodynamic thrust model, the force generated by an individual rotor depends on the thrust coefficient and the square of its rotational speed. Accordingly, the thrust can be mathematically formulated as follows:

$$U1 = 4b\omega^2 \qquad (18)$$

$$b = \frac{0.944\times9.8}{4\times1250^2} = 1.480 \times 10^{-6} kgm^2$$

4.1.5. Rotor Inertia

Equation (19) provides the mathematical representation of the rotor's moment of inertia.

$$\mathrm{J_r} = \frac{1}{2} \times m_r \mathrm{R}^2 \qquad (19)$$

$$\mathrm{J_r} = \frac{1}{2} \times (0.047 \times 0.215^2) = 1.086 \times 10^{-3} kgm^2$$

Where: m_r = mass of the motor = 0.047Kg and R= the dimension of the motor on the quadacopter axis=0.215m

4.1.6. Rotational dynamics

The rotational dynamics of the quadcopter are described by Euler's equations for a rigid body. These equations relate the body angular velocities to the applied control torques, external disturbance torques, and gyroscopic coupling effects. Assuming a diagonal inertia matrix, the rotational dynamics can be expressed as

$$I\dot{\omega} + \omega \times (I\omega) = \tau c + \tau d \qquad (20)$$

Where I=diag(I_{xx}, I_{yy}, I_{zz}) is the inertia matrix, ω=[p q r]T is the body angular velocity vector, $\tau_c = [\tau_\phi, \tau_\theta, \tau_\psi]$T represents the control torques, and= $[d_\phi, d_\theta, d_\psi]$T denotes the external disturbance torques.

Expanding (20) along the three body-fixed axes yields

$$I_{xx}\dot{p} + (I_{zz} - I_{yy})qr = \tau_\phi + d_\phi$$

$$I_{yy}\dot{q} + (I_{xx} - I_{zz})pr = \tau_\theta + d_\theta$$

$$I_{zz}\dot{r} + (I_{yy} - I_{xx})pq = \tau_\psi + d_\psi$$

Therefore, the angular accelerations are given by

$$\dot{p} = \frac{(I_{yy}-I_{zz})qr+\tau_\phi+d_\phi}{I_{xx}} \qquad (21.a)$$

$$\dot{q} = \frac{(I_{zz}-I_{xx})pr+\tau_\theta+d_\theta}{I_{yy}} \qquad (21.b)$$

$$\dot{r} = \frac{(I_{xx}-I_{yy})pq+\tau_\psi+d_\psi}{I_{zz}} \qquad (21.c)$$

For the commonly adopted ZYX Euler-angle convention, the relationship between the body angular velocity vector ω=[p q r]T and the Euler-angle rates is expressed as

$$\begin{bmatrix} p \\ q \\ r \end{bmatrix} = \begin{bmatrix} 1 & 0 & -sin\,\theta \\ 0 & cos\,\phi & sin\,\phi\,cos\,\theta \\ 0 & -sin\,\phi & cos\,\phi\,cos\,\theta \end{bmatrix} \begin{bmatrix} \dot{\Phi} \\ \dot{\theta} \\ \dot{\psi} \end{bmatrix}$$

$$p = \dot{\Phi} - \dot{\psi}\,sin\,\theta \qquad (22.a)$$

$$q = \dot{\theta}\,cos\,\phi + \dot{\psi} sin\phi\,cos\,\theta \qquad (22.b)$$

$$r = -\dot{\theta}\,sin\,\phi + \dot{\psi}\,cos\,\phi\,cos\,\theta \qquad (22.c)$$

By inverting the transformation matrix, the Euler-angle rates can be obtained as

$$\begin{bmatrix} \dot{\phi} \\ \dot{\theta} \\ \dot{\psi} \end{bmatrix} = \begin{bmatrix} 1 & sin\,\phi\,tan\,\theta & cos\,\phi\,tan\,\theta \\ 0 & cos\,\phi & -sin\,\phi \\ 0 & \frac{sin\,\phi}{cos\,\theta} & \frac{cos\,\phi}{cos\,\theta} \end{bmatrix} \begin{bmatrix} p \\ q \\ r \end{bmatrix}$$

Consequently,

$$\dot{\Phi} = p + q\,sin\,\phi\,tan\,\theta + r\,cos\,\phi\,tan\,\theta \qquad (23.a)$$

$$\dot{\theta} = q\,cos\,\phi - rsin\phi \qquad (23.b)$$

$$\dot{\psi} = \frac{qsin\,\phi+r\,cos\,\phi}{cos\,\theta} \qquad (23.c)$$

Differentiating these equations with respect to time gives the angular accelerations associated with the Euler angles. Under the small-angle approximation, where ϕ =0 and ψ=0, the kinematic relationships will simplified. In particular, differentiating Eq. (23.a) yields

$$\ddot{\Phi} = \dot{p} + \dot{q}sin\,\phi\,\tan\phi + \dot{r}\cos\phi\,\tan\theta + \dot{\Phi}(qcos\phi - rsin\phi)tan\theta + +(qsin\phi + rcos\phi)sec^2\,\theta\dot{\theta}$$

When ϕ =0, ψ=0

$$\ddot{\Phi} = \dot{p} + (rcos\phi)sec^2\,\theta\dot{\theta} \qquad (24)$$

Substitute (21.a) and (21.c) into (24), yields

$$\ddot{\Phi} = \frac{\dot{\theta}\dot{\psi}(I_{yy} - I_{zz}) + \tau_{\phi} + d_{\phi}}{I_{xx}}$$

$$\tau_{\phi} = I(U2)\,, \qquad d_{\phi} = J_r\dot{\theta}w$$

Hence,

$$\ddot{\Phi} = \frac{\dot{\theta}\dot{\psi}(I_{yy}-I_{zz})+J_r\dot{\theta}w+I(U2)}{I_{xx}} \qquad (25)$$

Differentiating Eq. (23.b) yields

$$\ddot{\theta} = \dot{q}cos\phi - \dot{r}sin\,\phi - \dot{\Phi}(qsin\phi + rcos\phi)$$

When ϕ =0 and ψ=0, yields

$$\ddot{\theta} = \dot{q} - \dot{\Phi}rcos\phi \qquad (26)$$

Substitute (21.b), (22.c) and (23.a) into (26), yields

$$\ddot{\theta} = \frac{\dot{\Phi}\,\dot{\psi}(I_{zz} - I_{xx}) + \tau_{\theta} + d_{\theta}}{I_{yy}}$$

$$\tau_{\theta} = I(U3), \qquad d_{\theta} = J_r\,\dot{\Phi}\,w$$

Hence,

$$\ddot{\theta} = \frac{\dot{\Phi}\,\dot{\psi}(I_{zz}-I_{xx})+J_r\,\dot{\Phi}\,w+I(U3)}{I_{yy}} \qquad (27)$$

Differentiating Eq. (23.c) yields

$$\ddot{\psi} = \frac{\dot{q}\,sin\phi + \dot{r}cos\phi}{cos\theta} + \frac{\dot{\Phi}(\mathrm{q}cos\phi - rsin\phi)}{cos\theta} + \frac{(\mathrm{q}sin\phi + rcos\phi)sin\theta}{cos^2\theta}$$

When ϕ =0 and ψ=0,

$$\ddot{\psi} = \dot{r} + \dot{\Phi}q \qquad (28)$$

Substitute (21.c), (22.b) and (23.a) into (28), yields

$$\ddot{\psi} = \frac{\dot{\theta}\,\dot{\Phi}\,(I_{xx} - I_{yy}) + \tau_{\theta} + d_{\theta}}{I_{zz}}$$

$$\tau_{\theta} = I(U4), \qquad d_{\theta}=J_r\,\dot{\Phi}\,w$$

$$\ddot{\psi} = \frac{\dot{\theta}\,\dot{\Phi}\,(I_{xx}-I_{yy})+I(U4)}{I_{zz}} \qquad (29)$$

4.1.7. Translational dynamics:

The linear acceleration can obtained depending in second newton law, equation (4).

The translational dynamics of the quadcopter are derived from Newton's second law, which states that the resultant external force acting on the vehicle equals its mass multiplied by its linear acceleration. Accordingly,

$$\ddot{r} = \frac{1}{m}\left[F_T^i + F_g + md\right] \qquad (30)$$

Where $r = [x, y, z]^T$ is the position vector in the inertial frame, (F_T) is the total thrust vector, (F_g) is the gravitational force, and (d) represents the equivalent external disturbances per unit mass.

The total thrust generated by the four propellers is defined as

$$U_1 = \sum_{i=1}^{4} F_i \qquad (31)$$

Where (F_i) denotes the thrust produced by the (i)-th propeller. The thrust vector is transformed from the body frame F_T^b to the inertial frame F_T^i using the rotation matrix determined by the Euler angles.

$$F_T^i = R^i F_T^b \qquad , F_T^b = \begin{bmatrix} 0 \\ 0 \\ U_1 \end{bmatrix}$$

$$F_T^i = \begin{bmatrix} (\sin\Phi \sin\psi) + (\cos\Phi \cos\psi \sin\theta) \\ (\sin\Phi \cos\psi) + (\cos\Phi \sin\psi \sin\theta) \\ (\cos\theta \cos\Phi) \end{bmatrix} U_1 \qquad (32)$$

By applying Newton's second law along the three inertial axes, the translational accelerations can be obtained as functions of the total thrust, vehicle orientation, gravity, and external disturbances.

$$\ddot{X} = \frac{(\sin\Phi \sin\psi)+(\cos\Phi \cos\psi \sin\theta)\mathrm{U1}-d_x}{m} \qquad (33)$$

$$\ddot{Y} = \frac{-(\sin\Phi \cos\psi)+(\cos\Phi \sin\psi \sin\theta)\mathrm{U1}-d_y}{m} \qquad (34)$$

$$\ddot{Z} = \frac{(\cos\theta\cos\Phi)\mathrm{U1} - (\mathrm{mg}) - d_z}{m} \qquad (35)$$

To simulate the quadcopter motion in both altitude and x-direction, a simplified translational dynamic model is considered by assuming the rolling angle, $\Phi = 0$ and yawing angle, $\psi = 0$, and pitching angel, $0 \leq \theta \leq 45^\circ$. Based on these assumptions, the system model is developed using Eq.(36) and (37) to simplify the control design and simulation process.

$$\ddot{X} = \frac{(\sin\theta)\mathrm{U1}}{m} + d_x \qquad (36)$$

Where d_x represents the aerodynamic disturbance in the x-direction, defined as

$$d_x = -\frac{A_x \dot{x}}{m}, \quad |d_x| \le \overline{d_x}, \quad \overline{d_x} = \frac{A_x}{m}\vartheta_x, max$$

Where A_x denotes the aerodynamic drag coefficient, and ϑ_x, max is the maximum velocity in the x-direction.

Similarly,

$$\ddot{Z} = \frac{(\cos\theta)\mathrm{U1}}{m} - g + d_z \qquad (37)$$

Where d_z represents the aerodynamic disturbance in the z-direction, defined as

$$d_z = -\frac{A_z \dot{z}}{m}, \quad |d_z| \le \overline{d_z}, \quad \overline{d_z} = \frac{A_z}{m}\vartheta_z, max$$

Where A_z denotes the aerodynamic drag coefficient, and ϑ_z, max is the maximum velocity in the z-direction.

4.2. Sliding Mode Controller Designing

A Sliding Mode Controller (SMC) is proposed to achieve robust altitude stabilization and trajectory tracking of the quadcopter in the presence of external disturbances. Specifically, the proposed SMC is designed to regulate the altitude z, track the square-path trajectory in the x-direction, and control the pitch angle θ. The tracking error vector is defined as

$$\begin{bmatrix} e_x \\ e_z \\ e_\theta \end{bmatrix} = \begin{bmatrix} x - x_d \\ z - z_d \\ \theta - \theta_d \end{bmatrix} \rightarrow \begin{bmatrix} e_x' \\ e_z' \\ e_\theta{}' \end{bmatrix} = \begin{bmatrix} x' - x_d' \\ z' - z_d' \\ \theta' - \theta_{d'} \end{bmatrix} \rightarrow$$

$$\begin{bmatrix} e_x'' \\ e_z'' \\ e_\theta'' \end{bmatrix} = \begin{bmatrix} x'' - x_d{}'' \\ z'' - z_d'' \\ \theta'' - \theta_d{}'' \end{bmatrix} \qquad (38)$$

Where the corresponding tracking errors are defined with respect to the desired trajectories. The sliding surfaces for the x-position, altitude, and pitch angle are selected as

$$\begin{bmatrix} s_x \\ s_z \\ s_\theta \end{bmatrix} = \begin{bmatrix} e_x' + \lambda_x e_x \\ e_z' + \lambda_z e_z \\ e_\theta' + \lambda_\theta e_\theta \end{bmatrix} \qquad (39)$$

Where λ_x, λ_z *and* λ_θ are positive design parameters that determine the convergence rate of the corresponding tracking errors.

Taking the time derivative of the sliding surfaces yields

$$\begin{bmatrix} s_x' \\ s_z' \\ s_\theta' \end{bmatrix} = \begin{bmatrix} e_x'' + \lambda_x e_x' \\ e_z'' + \lambda_z e_z' \\ e_\theta'' + \lambda_\theta e_z' \end{bmatrix} \qquad (40)$$

Substituting (38) into (40) gives

$$\begin{bmatrix} s_x' \\ s_z' \\ s_\theta' \end{bmatrix} = \begin{bmatrix} x'' - x_d'' + \lambda_x e_x' \\ z'' - z_d'' + \lambda_z e_z' \\ \theta'' - \theta_d'' + \lambda_\theta e_\theta' \end{bmatrix} \qquad (41)$$

By substituting the quadcopter dynamics given in (36) and (37) into (41), the sliding-surface dynamics can be expressed as

$$\begin{bmatrix} s_x' \\ s_z' \\ s_\theta' \end{bmatrix} = \begin{bmatrix} \frac{sin(\theta)U_1}{m} - x_d'' + \lambda_x e_x' + d_x \\ \frac{cos(\theta)U_1}{m} - g - z_d'' + \lambda_z e_z + d_z \\ \frac{I*U_3}{I_{yy}} - \theta_d'' + \lambda_\theta e_\theta' + d_\theta \end{bmatrix} \qquad (42)$$

The control input is designed according to the conventional SMC structure

$$u_{SMC} = u_{eq} + u_{sw} \qquad (43)$$

Where u_{eq} denotes the equivalent control component, which is responsible for maintaining the system motion on the sliding manifold, while u_{sw} denotes the switching control component, which drives the system trajectories toward the sliding manifold and provides robustness against bounded disturbances. To alleviate the chattering phenomenon associated with the discontinuous switching term, the conventional sign function is replaced by a saturation function. This modification improves the smoothness of the control input while preserving the robustness characteristics of the sliding-mode controller.

The equivalent control component is obtained by imposing the ideal sliding condition

$$s_i = 0, \qquad s_i' = 0,$$

Where $i \in \{x, z, \theta\}$. Therefore, setting the derivative of each sliding surface to zero and solving for the corresponding control input yields

$$\begin{bmatrix} s_x' \\ s_z' \\ s_\theta' \end{bmatrix} = \begin{bmatrix} \frac{sin(\theta)\, U_{eq,x}}{m} - x_d'' + \lambda_x e_x' \\ \frac{cos(\theta)\, U_{eq,z}}{m} - g - z_d'' + \lambda_z e_z \\ \frac{I * U_{eq,\theta}}{I_{yy}} - \theta_d'' + \lambda_\theta e_\theta' \end{bmatrix} = \begin{bmatrix} 0 \\ 0 \\ 0 \end{bmatrix} \rightarrow$$

$$\begin{bmatrix} U_{eq,x} \\ U_{eq,z} \\ U_{eq,\theta} \end{bmatrix} = \begin{bmatrix} \frac{m}{sin(\theta)}(x_d'' - \lambda_x e_x') \\ \frac{m}{cos(\theta)}(g + z_d'' - \lambda_z e_z) \\ \frac{I}{I_{yy}}(\theta_d'' - \lambda_\theta e_\theta') \end{bmatrix} \quad (44)$$

The switching control component is selected as

$$u_{sw,i} = -k_i sat\left(\frac{s_i}{\emptyset_i}\right) \quad \rightarrow$$

$$\begin{bmatrix} U_{sw,x} \\ U_{sw,z} \\ U_{sw,\theta} \end{bmatrix} = \begin{bmatrix} \frac{-mk_x}{sin(\theta)} sat(\frac{s_x}{\emptyset_x}) \\ \frac{-mk_z}{cos(\theta)} sat(\frac{s_z}{\emptyset_z}) \\ \frac{-Ik_\theta}{I_{yy}} sat(\frac{s_\theta}{\emptyset_\theta}) \end{bmatrix} \quad (45)$$

Where $k_i > 0$ denotes the sliding-mode gain and $\emptyset_i > 0$ represents the boundary-layer thickness associated with the saturation function. Substituting the switching control law (45) into the sliding-surface dynamics (42) yields the following closed-loop sliding dynamics:

$$\begin{bmatrix} s_x' \\ s_z' \\ s_\theta' \end{bmatrix} = \begin{bmatrix} -k_x sat\left(\frac{s_x}{\emptyset_x}\right) + d_x \\ -k_z sat(\frac{s_z}{\emptyset_z}) + d_z \\ -k_\theta sat\left(\frac{s_\theta}{\emptyset_\theta}\right) + d_z \end{bmatrix} \quad (46)$$

These closed-loop dynamics form the basis for the subsequent Lyapunov stability and robustness analysis.

4.3. Stability of the Controlled System

To analyze the stability of the proposed closed-loop control system, the following positive-definite Lyapunov candidate function is selected:

$$V = \frac{1}{2}(S_x^2 + S_z^2 + S_\theta^2) \quad (47)$$

where S_x, S_z, and S_θ denote the sliding variables associated with the x-position, altitude, and pitch-angle tracking errors, respectively. Clearly,

$$V > 0, \quad \rightarrow \quad S \neq 0,$$

And

$$V = 0, \quad \rightarrow \quad S = 0,$$

Where

$$S = [S_x \;\; S_z \;\; S_\theta]^T$$

Therefore, V is positive definite with respect to the sliding-variable vector S.

The rate of change of the Lyapunov function, evaluated along the closed-loop system trajectories, can be expressed as follows:

$$\acute{V} = S_x\acute{S_x} + S_z\acute{S_z} + S_\theta\acute{S_\theta} \qquad (48)$$

Substituting (46) into (48) gives

$$\acute{V} = -k_x S_x sat\left(\frac{S_x}{\emptyset_x}\right) - k_z S_z sat\left(\frac{S_z}{\emptyset_z}\right) - k_\theta S_\theta sat\left(\frac{S_\theta}{\emptyset_\theta}\right) + S_x d_x + S_z d_z + S_\theta d_\theta \qquad (49)$$

Assume that the aerodynamic disturbances are bounded, such that

$$|d_x| \leq \overline{d_x}, \qquad |d_z| \leq \overline{d_z}, \quad |d_\theta| \leq \overline{d_\theta} \qquad (50)$$

Outside the boundary layer, i.e., for$|S_i| > \emptyset_i$, the saturation function satisfies

$$\because sat\left(\frac{s_i}{\emptyset_i}\right) = sign(S_i)$$

Therefore,

$$S_i sat\left(\frac{S_i}{\emptyset_i}\right) = |S_i|$$

Furthermore, since $s_i d_i \leq |s_i||d_i| \leq |s_i|\overline{d_\iota}$,

The derivative of the Lyapunov function satisfies

$$\acute{V} \leq -k_x|S_x| - k_z|S_z| - k_\theta|S_\theta| + \overline{d_x}|S_x| + \overline{d_z}|S_z| + \overline{d_\theta}|S_\theta|$$

$$\acute{V} \leq -(k_x - \overline{d_x})|S_x| - (k_z - \overline{d_z})|S_z| - (k_\theta - \overline{d_\theta})|S_\theta| \qquad (51)$$

Hence, by selecting the sliding-mode gains such that

$$k_x > \overline{d_x}, \quad k_z > \overline{d_z}, \quad k_\theta > \overline{d_\theta} \qquad (52)$$

It follows that

$$\dot{V} < 0, \qquad s \neq 0 \quad (53)$$

5. Simulation Setup and Results Discussion

The proposed Sliding Mode Controller (SMC) was implemented in MATLAB/Simulink to evaluate the altitude stabilization and trajectory tracking performance of the quadcopter under model uncertainties and external disturbances (air resistance). The controller was designed based on the nonlinear quadcopter dynamics, while the same reference trajectory and simulation conditions were used for both the SMC and PID controllers to ensure a fair performance comparison. Amore detailed description of the simulation model shown in Fig.3 can be found in [5].

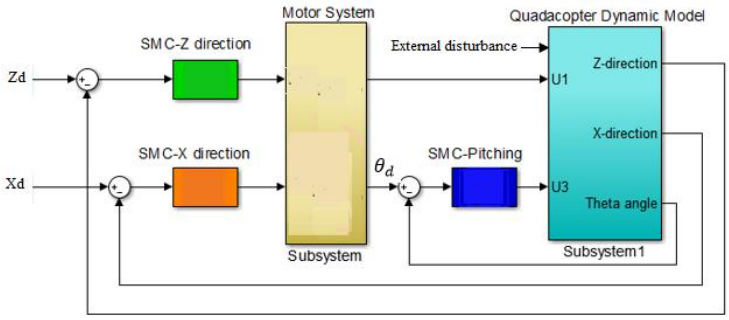


Fig. 3: SMC for quadcopter simulation model.

Fig. 4 presents the altitude response of the proposed SMC. The quadcopter reaches the desired altitude of 3 m with a smooth transient response, limited overshoot, and stable steady-state behavior.

The corresponding tracking error shown in Fig. 5 gradually converges to zero, indicating accurate altitude regulation and effective disturbance rejection.

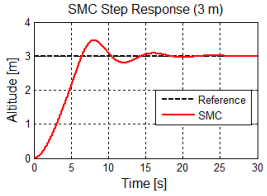


Fig.4: quadcopter altitude response of SMC system.

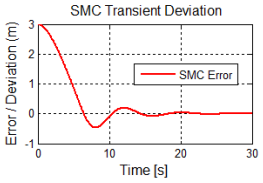


Fig.5: error deviation of quadcopter altitude system.

Fig.6 and Fig.7 illustrate the acceleration and velocity responses along the altitude axis. Both variables converge to zero after the transient period, confirming stable hovering conditions and the absence of residual oscillations at steady state.

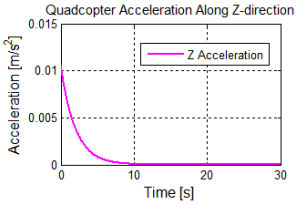


Fig.6: decreasing acceleration to zero means altitude stabilization.

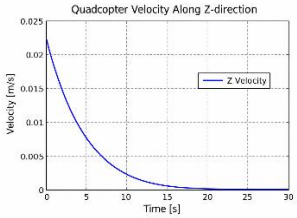


Fig.7: decreasing velocity until reaching preset

A comparison between the SMC and the conventional PID controller is presented in Fig.8. The proposed SMC exhibits faster convergence, reduced oscillations, and improved robustness compared with the PID controller. The altitude tracking error shown in Fig.9 decreases more rapidly under the SMC, demonstrating its superior tracking accuracy

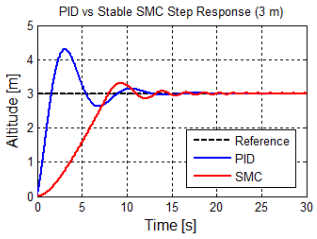


Fig.8: comparison performance of PID and SMC.

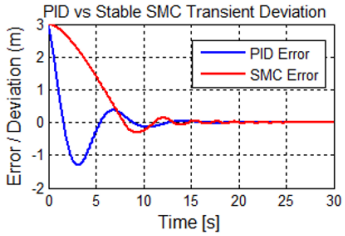


Fig.9: error altitude deviation of PID and SMC.

The tracking performance along the x -direction is shown in Fig.10. The proposed SMC accurately follows the prescribed step reference while maintaining a fast transient response and negligible steady-state error. In contrast, the PID controller exhibits slower convergence and larger deviations during reference changes. The corresponding tracking errors are presented in Fig.11, where the SMC consistently achieves lower tracking errors than the PID controller.

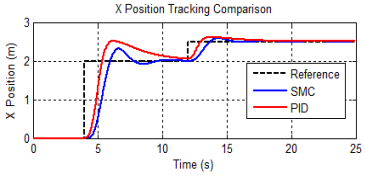


Fig. 10. Position tracking performance in the x-direction.

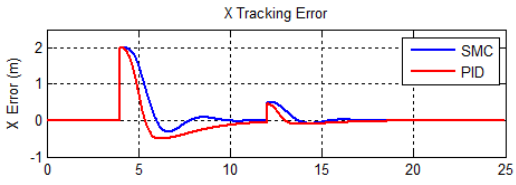


Fig.11. error deviation of quadcopter in the X-direction of PID and SMC.

The altitude tracking comparison during the complete mission is illustrated in Fig.12. The proposed SMC successfully regulates the altitude during both ascending

and descending maneuvers with fast convergence and limited overshoot. The corresponding altitude tracking error shown in Fig.13 confirms the improved accuracy of the SMC compared with the PID controller.

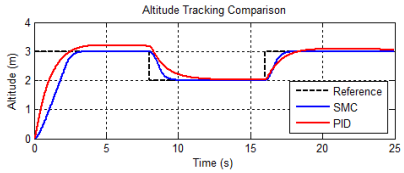


Fig. 12. Altitude tracking response of the quadcopter.

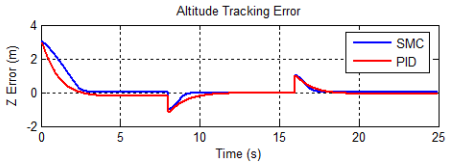


Fig. 13. Altitude tracking error of the quadcopter.

The pitch angle response generated by the proposed controller is shown in **Fig14**. The pitch angle remains within acceptable operating limits and changes smoothly during horizontal motion to generate the required translational force before returning to its equilibrium value.

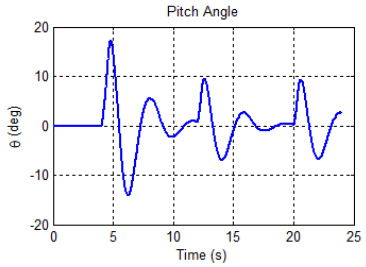


Fig.14. Pitch angle response during trajectory tracking.

The total thrust generated by the controller is illustrated in Fig.15. The thrust input varies according to the altitude and trajectory requirements while remaining bounded throughout the simulation, ensuring stable flight performance.

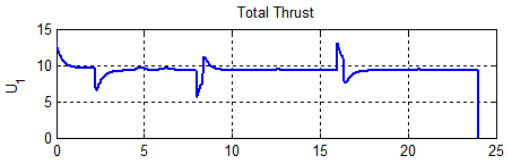


Fig.15. Total thrust control input U1.

Fig.16 presents the pitch control torque. The controller generates the required corrective torque during attitude adjustments while maintaining a smooth and bounded control signal, which contributes to stable attitude regulation.

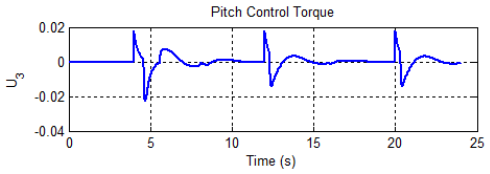


Fig.16. Pitch control torque U3.

The actual and desired trajectories in the $x-z$ plane are compared in Fig.17. The proposed SMC closely follows the reference trajectory with only small deviations during transition intervals, confirming accurate trajectory tracking and stable flight performance.

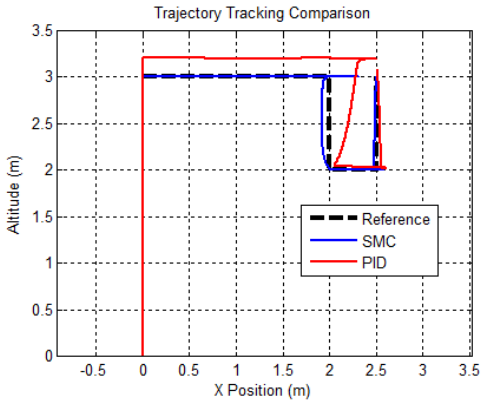


Fig.17. Actual and desired trajectory of the quadcopter in the X–Z plane.

The acceleration responses of both controllers are compared in Fig.18. The SMC exhibits a faster transient response with well-controlled acceleration profiles, whereas the PID controller shows slower dynamic behavior during reference changes.

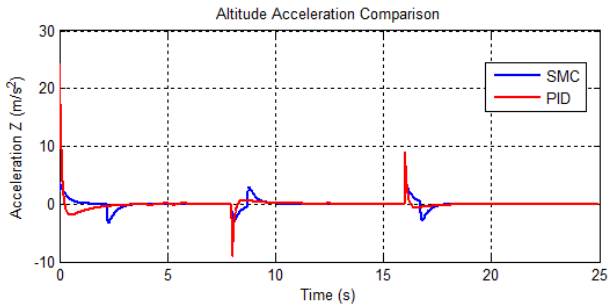


Fig.18.SMC and PID acceleration comparison.

The velocity responses in the X- and Z-directions are presented in Fig.19 and Fig.20, respectively. In both directions, the SMC reaches the desired motion more rapidly and settles faster than the PID controller, demonstrating improved dynamic performance and enhanced tracking capability.

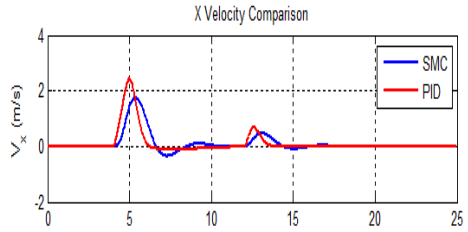


Fig.19. SMC and PID velocity comparison in x the direction.

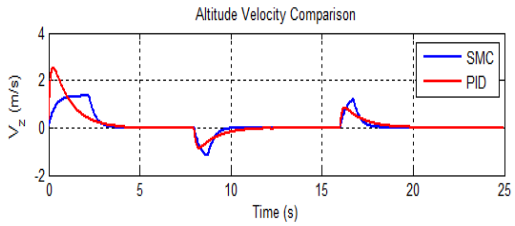


Fig.20. SMC and PID velocity comparison in the z direction.

Table 2 summarizes the performance comparison between the proposed Sliding Mode Controller (SMC) and the conventional PID controller. The results indicate that the PID controller provides a faster initial response and lower average tracking error, as reflected by the lower rise time, RMSE, and ISE values. In contrast, the SMC achieves a shorter settling time, eliminates overshoot, and exhibits negligible steady-state error, demonstrating superior tracking accuracy after the transient phase. Furthermore, the lower IAE and ITAE values obtained by the SMC indicate a reduced accumulated tracking error and faster attenuation of persistent errors over time. Overall, the results demonstrate the expected trade-off between the two control strategies: the PID controller offers smoother transient performance, whereas the proposed SMC provides higher steady-state accuracy and stronger robustness, making it more suitable for precision trajectory-tracking applications.

Table 2: Performance comparison.

Performance Index	PID	SMC	% improvement
Rise Time(s)	1.820	2.380	PID 23%
Settling Time(s)	24.870	17.380	SMC 30%
Maximum Overshoot (%)	6.94	0.00	SMC 100%
Steady-state Error X (m)	0.00105	0.00008	SMC 92%
Steady-state Error Z (m)	0.06260	0.00000	SMC 100%

RMSE X (m)	0.37825	0.43339	PID 13%
RMSE Z (m)	0.50307	0.64256	PID 22%
ISE	9.8589	14.9729	PID 34%
IAE	10.4168	9.7975	SMC 6%
ITAE	74.5055	48.8534	SMC 34%

6. Conclusion

This paper presented the design and evaluation of a Sliding Mode Controller (SMC) for quadrotor stabilization and trajectory tracking in the X–Z plane. The proposed controller was evaluated using a Newton–Euler-based quadrotor model through MATLAB simulations under various reference trajectory scenarios. The obtained results demonstrated the capability of the SMC to achieve accurate trajectory tracking with high steady-state precision and robust stabilization performance under nonlinear quadrotor dynamics.

A comparative evaluation with a conventional PID controller showed that both control strategies successfully tracked the desired trajectories while exhibiting different performance characteristics. The PID controller provided smoother transient behavior, whereas the SMC demonstrated faster convergence, lower steady-state error, and enhanced robustness against nonlinear system behavior. Furthermore, the use of a saturation function in the sliding surface effectively reduced the chattering phenomenon and improved the smoothness of the control signals.

Overall, the simulation results confirm that the proposed SMC provides an effective and reliable solution for quadrotor trajectory tracking applications requiring high accuracy and robustness a. Further research will be directed toward validating the proposed approach through practical experiments on a physical quadrotor platform. In addition, the controller will be evaluated under realistic operating scenarios to assess its ability to cope with external disturbances, sensor measurement noise, and uncertainties in system parameters.

References

[1] C. V. Nguyen, M. T. Nguyen, H. T. Tran, M. L. Trinh, H. M. La, and H. T. T. Nguyen, "Trajectory Tracking Control for a Quadcopter under External Disturbances," Engineering,

Technology & Applied Science Research, vol. 14, no. 6, pp. 17620–17628, 2024, doi: 10.48084/etasr.8449.

[2] T. L. Mien and V. Duy, "The Altitude and Position PID Controllers Design for UAV Quadcopter: From Theory to Experiment," Journal of Measurement, Control and Automation, vol. 29, no. 3, pp. 23–32, Oct. 2025, doi: 10.64032/mca.v29i3.318.

[3] X. Wu, Y. Pan, Q. Chen, N. Zheng, and Z. Chen, "Attitude Control of a Quadcopter UAV Using Sliding Mode Control with an Improved Extended State Observer," Electronics, vol. 14, no. 22, p. 4416, 2025, doi: 10.3390/electronics14224416.

[4] Z. Rakhman and A. Arkham, "Robust Control of a Quadcopter Flying via Sliding Mode," Journal of Science and Application Technology, 2024, doi: 10.35472/281446.

[5] K. A. E. Husain, M. A. Mahmoud, M. M. Essa, and M. A. Shtewi, "Control of Quadcopter Altitude Using PID Controller," Libyan Open University Journal of Applied Sciences (LOUJAS), vol. 2, no. 1, pp. 137–153, 2026.

[6] M. R. Chughtai, M. L. Anjum, I. Ahmad, M. Iqbal, D. Almakhles, and M. Abdelrahim, "Trajectory Tracking Control Design for Quadcopter Based on Optimized Integral Super-Twisting Sliding Mode Technique," Engineering Science and Technology, an International Journal, vol. 72, p. 102222, 2025, doi: 10.1016/j.jestch.2025.102222.

[7] N. P. Nguyen, N. X. Mung, H. L. N. N. Thanh, and S. K. Hong, "Adaptive Sliding Mode Control for Attitude and Altitude System of a Quadcopter UAV via Neural Network," IEEE Access, 2021, doi: 10.1109/ACCESS.2021.3064883.

[8] M. Maaruf, A. N. Abubakar, and M. M. Gulzar, "Adaptive Backstepping and Sliding Mode Control of a Quadrotor," Journal of the Brazilian Society of Mechanical Sciences and Engineering, vol. 46, p. 630, 2024, doi: 10.1007/s40430-024-05188-z.

[9] F. Serrano, O. Castillo, M. Alassafi, F. Alsaadi, and A. Ahmad, "Terminal Sliding Mode Attitude-Position Quaternion Based Control of Quadrotor Unmanned Aerial Vehicle," Advances in Space Research, 2023, doi: 10.1016/j.asr.2023.02.030.